Chapter 6. The effect of surfactants on the photovoltaic properties of hybrid bulk heterojunction solar cells based on MEH-PPV and TiO_2-based materials

Thi Thuy Duong Vu [a,b], *Frej Mighri* [a,b,*], *Trong-On Do*[a,c] *Abdellah Ajji*[b,d],

[a]Department of Chemical Engineering, Laval University, Quebec, QC, G1V 0A6 Canada;

[b] Center for Applied Research on Polymers and Composites (CREPEC);

[c]Centre in Green Chemistry and Catalysis (CGCC);

[d]Department of Chemical Engineering, École Polytechnique of Montreal, C.P. 6079, Montreal, QC, H3C 3A7 Canada.

Will be appeared in Green Processing and Synthesis Journal, 2015 March.

Abstract

In this work, we present the synthesis details of uniform shape and size-controlled titanium dioxide (TiO_2) nanorods followed by the deposition of cadmium sulfide (CdS) quantum dots on their surface. The achieved surfactant-capped-TiO_2 nanorods as well as CdS/TiO_2 nanocomposites were dispersed in nonpolar solvents, which enabled an easy solution blending with MEH-PPV conjugated polymer to prepare the active layer of bulk heterojunction solar cells (BHJSCs). The properties of the synthesized capped-TiO_2 nanorods, CdS/TiO_2 nanocomposites, as well as those of their corresponding blends with MEH-PPV were characterized using transmission electron microscopy (TEM), thermogravimetric analysis (TGA), UV-Visible spectroscopy, and Photoluminescence (PL) technique. The characterization of the effect of the surfactants (oleic acid, OA, olyamine, OM, and 6-aminohexanoic acid, 6AHA) left on TiO_2 surface and CdS surface modification on BHJSC photovoltaic power conversion efficiency (PEC) showed that: i) for the same surfactants, when CdS was added on the surface of TiO_2 nanorods, the PEC increased due to the higher efficiency of CdS compared to MEH-PPV; and ii) the best PEC was obtained with CdS/OA-6AHA-capped-TiO_2 nanocomposite due to the shortest length of the carbon-chain of 6AHA, leading higher charge carrier mobility.

Résumé

Dans ce travail, on démontre la synthèse des nanotiges de dioxide de titanium avec une forme uniforme et une taille contrôlée suivie d'une déposition des points quantiques des CdS sur leurs surfaces. Les capsules de nanotiges du surfactant TiO_2 et les nanocomposites CdS/TiO_2 peuvent être dispersé dans un solvant non polaire ce qui facilite la préparation d'une couche active pour une hétérojonction du mélange (BHJ) des piles solaires. Ces dernières comprennent MEH-PPV et des capsules de nanotiges du surfactant TiO_2 et les nanocomposites CdS/TiO_2. Les propriétés des nanotiges TiO_2 recouvert en surfactants et composites de CdS/TiO_2 ainsi que les propriétés de leurs mélanges avec MEH-PPV ont été caractérisées par la microscopie électronique à transmission (TEM), l'analyse thermogravimétrique (TGA), la spectroscopie UV-Visible et la technique de photoluminescence (PL). La caractérisation du l'effet de la déposition des CdS et des surfactants (acide oléique, olyamine et acide 6-aminohexanoïque) sur la surface de TiO_2 sur l'efficacité de conversion de BHJSC photovoltaïque a montré que : i) Pour la même surfactant, l'addition de CdS sur la surface des nanotiges de TiO_2 a augmenté la PEC due à la grande efficacité de CdS par rapport à celle de MEH-PPV; et ii) le meilleur PEC a été obtenu avec les nanocomposites de TiO_2 recouverts par CdS/OA-6AHA due à la longueur le plus court de chaine de carbone de 6AHA entrainant la plus haute mobilité des particules chargées.

6.1. Introduction

Over the last decade, hybrid bulk heterojunction solar cells (BHJSC) using soluble conjugated polymers and inorganic nanoparticles have become attractive for use as large area, physically flexible and low-cost solar cells.[1-3] Conjugated polymers can exhibit both electronic and optical properties, and they are well known for their mechanical properties and intrinsic processing advantages, which makes the fabrication of BHJSCs easy leading to a low manufacturing cost. However, conjugated polymers have low mobility of charge carriers, particularly electrons, which results in insufficient charge generation and transportation. Therefore, the introduction of inorganic nanomaterials into polymer matrix would further increase the performance and the efficiency of the organic solar cell by using the high electron mobility of the inorganic phase. Currently, the most common conjugated polymers used as hole transporting materials in solar cells are poly (2-methoxy, 5-(2-ethyl-hexy-loxy)-p-phenyl vinylene) (MEH-PPV),[4-7] poly(3-hexylthiophene) (P3HT),[8,9] and poly(2-methoxy-5-(3,7-dimethyloctyloxy)-1,4-phenylene-vinylene) (MDMO-PPV);[9] while different types of inorganic nanoparticles and nanoparticle system are an example of materials used such as CdS,[4] CdTe,[7,10] CdSe,[11,12] ZnO,[13-15] TiO_2,[16-18] CdSe-CdTe,[19] PbS/TiO_2 have been reported.[20]

Due to the difference of electrical and optical properties of the two materials, the photogenerated excitons can diffuse to the interface between the conjugated polymer and the inorganic nanomaterials, but the charge transportation through the nanocrystalline network can be strongly affected by surface defects and adsorbed species on nanocrystals surface, which acts as surface traps. Therefore, these traps can affect the mobility of charge carriers and probably can cause their recombination, thus they affect the power efficiency conversion (PEC) of the solar cells. Therefore, by controlling particle crystallinity as well as their surface properties, we could help to enhance the PEC of BHJSCs.

In this work, we present a simple low temperature solvothermal synthesis process to develop surfactant-capped-TiO_2 nanorods using different capping surfactants. The shape and size of these TiO_2 nanorods were controlled and optimized in nano-scale range for BHJSC application. We also present a facile method for developing CdS/TiO_2 collide systems using the above developed capped-TiO_2 nanorods. As a final step, both capped-

TiO_2 nanorods and CdS/TiO_2 nanocomposites were separately blended with MEH-PPV polymer. Blend solution was used to develop the active layer of BHJSC prototypes by using the spin-coating method at room temperature. The photovoltaic properties of these prototypes were then characterized and the effect of TiO_2 surface modification on these properties was studied.

6.2. Experimental

6.2.1. Materials

Commercially titanium (IV) butoxide (TB, 97%), oleic acid (OA, 90%), oleyl amine (OM, 70%), 6-aminohexanoic acid (6AHA), cadmium acetate dehydrate, thioamide, nitrosonium tetrafluoroborate solution ($NOBF_4$) and 2-methoxy-5-(2'-ethylhexyloxy)-p-phenylene vinylene (MEH-PPV) (PS-3900) with the average molecular weight of 150,000-250,000 were purchased from Sigma - Aldrich Chemical, Canada. Poly(3,4-ethylenedioxythiophene) poly(styrenesulfonate) (PEDOT:PSS) and Indium-tin-oxide (ITO) glass substrate 25x25 mm were respectively purchased from Nova Chemical and Merck, Canada. Absolute (pure) ethanol (EtOH), from Brampton, Canada, N,N-dimethylformamide (DMF), dichloromethane, dichlorobenzyl, and hexane, from Fisher Scientific, Canada, and toluene, from Anachemia Canada Inc., were all of analytical grade. All chemicals were used as received without further purification or distillation.

6.2.2. Synthesis of OA and OM or 6-AHA Capped TiO_2 nanorods

OA, OM or 6AHA capped anatase TiO_2 nanorods were synthesized at low temperature by the hydrolysis of TB using OA and OM or 6AHA as surfactants followed by the steps that we already described in our previous work.[21, 22] Typically, 1 mmol of TB was added to a mixture of 7 mmol of OA, 3 mmol of OM or 6AHA, and ethanol. The system was then heated at 140°C for 18 h. The resulting TiO_2 nanocrystals were washed with toluene and ethanol 95% several times then dried at room temperature.

6.2.3. Synthesis of CdS modified TiO_2 nanocomposite

It is important to mention that the use of surfactants during the synthesis of TiO_2 nanorods results in the presence of capping molecules on the surface of these nanorods. These capping molecules create an insulating barrier around each nanorod and block the access to its surface. Therefore, in order to deposit CdS nanoparticles on the surface of TiO_2 nanorods, the latter must undergo a surface treatment, typically by replacing the original ligands with specifically designed species through a ligand-exchange process. For this, $NOBF_4$ was used in our study. This strategy helps to enable sequential surface modification of TiO_2 nanorods without affecting their size and shape, and also to increase the access to their surface.

Basically, surfactants-capped-TiO_2 nanorods dispersed in hexane solvent were added into 5 mL of dichloromethane solution of $NOBF_4$ (0.01M). The mixture was well shaken; the precipitation of TiO_2 nanorods was then observed just after few minutes. Precipitated nanorods were collected then washed by using a mixture of toluene and ethanol 95%.

As a final step, 4.5 mmol of the above treated TiO_2 nanorods were dispersed in 10 ml of DMF and 9 mmol of cadmium acetate dihydrate then stirred under room temperature for 2 h. Subsequently, 9 mmol of thioamide were added to the mixture and let under stirring overnight. The precipitated CdS/TiO_2 nanocrystals were washed few times using toluene and ethanol 95%, and then collected by centrifugation.

6.2.4. Preparation of MEH-PPV/capped-TiO_2 and MEH-PPV/CdS/TiO_2 blend solutions

Mixtures of MEH-PPV and TiO_2 or CdS/TiO_2 were prepared by solution blending in dichlorobenzyl solvent with a mole ratio MEH-PPV:TiO_2 or MEH-PPV:CdS/TiO_2 of 1:3. Blend solutions were continuously stirred overnight under dark. Ultrasonic agitation was applied to disperse nanoparticle agglomerates in the solvent and to ensure dispersion homogeneity.

6.2.5. Fabrication of BHJ solar cell devices

The fabrication process consists to develop a sandwich structure, as shown in scheme 1, composed of i) ITO/PEDOT:PSS anode, ii) MEH-PPV/CdS/TiO_2 nanocomposite active layer, and iii) Al cathode.[23] A 25x25 mm ITO glass substrate with a sheet resistance of 15Ω/square was ultrasonically cleaned with soap, followed by acetone then isopropanol solvents. A thin layer of PEDOT:PSS was then spin-coated on the cleaned ITO glass substrate, then baked at 80ºC for 5 min to remove any possible contamination. Being a highly hole-conducting metal-like polymer, PEDOT:PSS eases the conduction of holes from the active layer to the ITO layer by lowering the intrinsic energetic barrier between the ITO work function and the HOMO of the active material. So this layer acts as a semi-permeable membrane for holes only and blocks the extraction of electrons on the ITO side. Therefore, PEDOT:PSS layer helps to reduce electron-hole recombination phenomena. In addition, it also allows ITO surface smoothing, which is usually quite rough, and hence reduces the risks of shortcuts within the BHJSC. The composite CdS/TiO_2/MEH-PPV solution already prepared, which constitutes the active layer, was then deposited over the PEDOT:PSS layer by the same spin-coating technique. Finally, four aluminum cathode layers (700 Å in thickness) were then thermally evaporated in vacuum chamber at a pressure below 3 x 10^{-4} Pa. The final device is then composed of four heterojunction cells with individual active area of 0.24 cm^2.

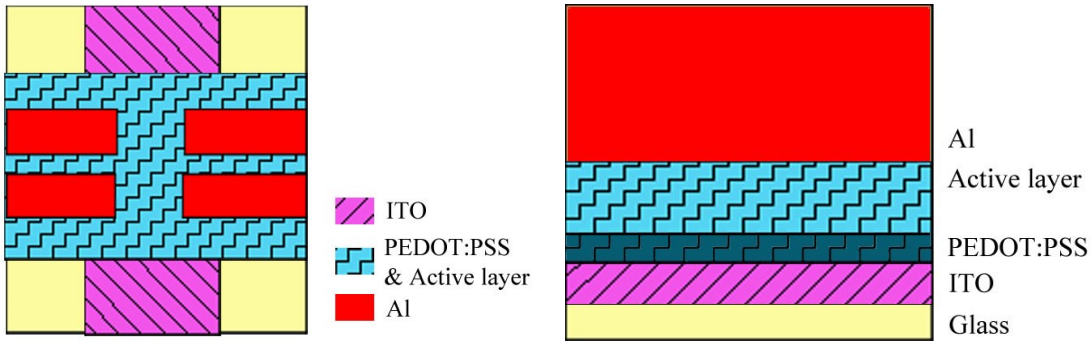

Scheme 6.1. Architecture scheme of a BHJSC device

6.2.6. Characterization

Powder X-ray diffraction (XRD) characterization was done using a Bruker SMART APEXII X-ray diffractometer equipped with a Cu Kα radiation source (λ = 1.5418 Å) in the 2θ range of 5–20° at a scan rate of 1.0°/min. All samples were dried at 65°C overnight to eliminate guest solvent molecules on the surface of particles before the XRD scan. Fourier transform infrared (FTIR) characterization was done using a FTS 45 infrared spectrophotometer in the spectral range of 4000–400 cm^{-1}. The characterization was done at room temperature using atmosphere as background. The thermal characterization of the developed TiO_2 nanorods, CdS nanoparticles and hybrid CdS/TiO_2 nanocomposites was carried out at a heating rate of 10°C/min up to 900°C under an oxygen flow using a Perkin-Elmer TGA thermogravimetric analyzer. The UV−visible spectra of the developed nanostructures were recorded on powder samples using a Cary 300 Bio UV−visible spectrophotometer; pure toluene was used as a blank. Room temperature photoluminescence (PL) characterization was done by using an optical spectrum analyzer (ANDO AQ6317, Japan). Electronic transport in the BHJSC device was studied via current density-voltage (I-V) characterization using a 2400 Keithley source meter. The voltage was varied from -0.5 to 2.0 V. I-V curves were taken both in the dark and under white illumination provided by a halogen source through the ITO electrode.

6.3. Results and Discussions

6.3.1. Analysis of synthesized capped-TiO_2 nanorods

6.3.1.1. TEM Characterization

Figures 6.1(a) and (b) show representative TEM images of the as-synthesized TiO_2 nanoparticles using respectively OA/OM and OA/6AHA as surfactant combinations. In both cases, the shape of TiO_2 nanoparticles was in the form of nanorods of 4–5 nm in diameter and 20–40 nm in length. The morphologies of TiO_2 nanoparticles were closely controlled by the presence of OA/OM and OA/6AHA surfactants. According to literature,

these surfactants play important roles during the hydrolysis process as they generate water resulting from the acid-base pair catalyst. More they generate water, faster is the hydrolysis process, leading to larger nanoparticle dimensions. Besides, the presence of surfactant lowers the surface tension, which allows particles further grow in surfactant direction. For the case of addition of TB precursors into the reaction solution, the early formation of TiO_2 truncated octahedral bi-pyramid seeds were expected. These seeds terminated by {001} faces, which have high surface energy, and {101} faces with relative low energy. When the hydrolysis process increases, the final shape of TiO_2 nanoparticles is more controlled by the competition between the relative surface energies of the {001} and {101} faces and, therefore, the growth rate ratio between [001] and [101] directions.[21, 24-26] Hence, with the utilization of OA surfactant, which is more favored to bind strongly to TiO_2 {001} faces, and amines like OM or 6AHA that weakly bind on {101} faces, this leads to a more progressive TiO_2 growth along [001] direction than along [101] direction. Therefore, this oriented growth leads to TiO_2 nanorods instead of TiO_2 nanospheres or nanorhombics, as presented in our previous work.[21]

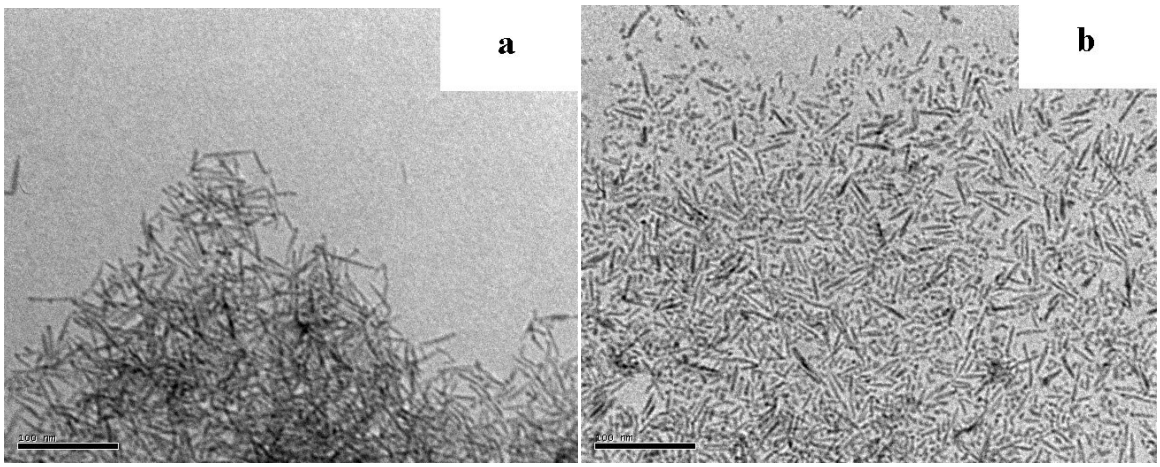

Figure 6.1. TEM of TiO_2 nanorods synthesized using (a) OA/OM, and (b) OA/6AHA surfactants combinations

6.3.1.2. XRD and FTIR characterization

Figure 6.2 shows XRD spectra of OA/OM-capped-TiO_2 and OA/6AHA-capped-TiO_2 nanoparticles. Both spectra show strong diffraction peaks at 25° and 48°, indicating

TiO_2 anatase phase with typical anisotropic growth pattern along the [001] direction (JCPDS no: 88-1175 and 84-1286). In order to understand the surface properties of TiO_2 nanorods, FTIR characterization was carried out. The FTIR of pure OA, OM, and 6AHA surfactants were also analyzed for comparison. The corresponding results are shown in Figure 6.3. The FTIR bands at 2850-2920 cm^{-1} are attributed to the asymmetric and symmetric C–H stretching vibrations of methylene groups, the vibration at 1465 cm^{-1} is a characteristic of $-(CH_2)_n-$ chains with $n > 3$, the small peaks at 3004 cm^{-1} correspond to the stretching of =C-H bond.[27-29] Furthermore, it was observed that the vibration bands at 1710 and 1285 cm^{-1}, which are the characteristic bands of carbonyl -C=O- and -C-O- stretch in the carboxyl acid of OA, appear weak on the spectrum (A2) of OA-6AHA-capped-TiO_2 nanoparticles and that of OA-OM-capped-TiO_2 nanoparticles (A1). This indicates in both cases chemisorptions of oleic acid onto the surface of TiO_2 nanorods.[30] However, the intensities of those absorption bands are all reduced compared to the absorption bands of pure OA, OM and 6AHA. This is due to the fact that only small amounts of surfactants are expected to be left on the surface of TiO_2 nanoparticles. Also, the FTIR spectrum (A1) of OA-OM-capped-TiO_2 nanoparticles shows a vibration band at 1379 cm^{-1}, which is identical to that observed on the FTIR spectrum of pure OM.[31] This indicates the presence of OM on the surface of OA-OM-capped-TiO_2 nanoparticles. A close look to the spectrum shows two peaks at 1536 and 1560 cm^{-1} corresponding to the symmetric and asymmetric stretching vibrations of uncoordinated –COO- group.[32] These two peaks are observed to be absent on the spectrum (A2) of OA-6AHA-capped-TiO_2 nanoparticles. The latter spectrum also shows a band at 1386 cm^{-1} corresponding to C–N stretching mode of AHA molecules, and two vibration peaks at 1622 and 1506 cm^{-1}, which are anti-symmetric and symmetric deformation peaks of NH_3^+. These results prove the binding of amino groups on the surface of TiO_2 nanorods and show that i) only the amino ($–NH_2$) group of AHA molecules capped on the surface of TiO_2 nanorods and ii) the free carboxylic (–COOH) terminus was oriented outward.[33] Finally, the broad band at around 3000 to 3600 cm^{-1} is due to the presence of adsorbed water on surface of the sample. This band also appears on spectrum (A1) of OA-OM-capped- TiO_2 nanoparticles but with a lower intensity, which is an indication that the amount of water on OA-OM-capped- TiO_2 was less than that on OA-6AHA-capped- TiO_2. This will also be confirmed in by TGA characterization presented in the following section.

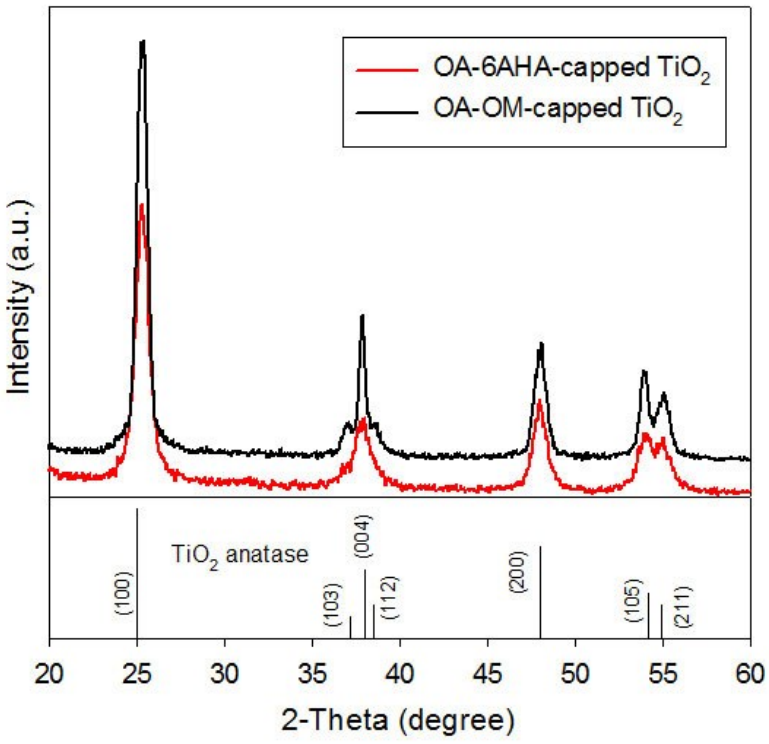

Figure 6.2. Powder XRD patterns of OA-OM-capped-TiO_2 and OA-6AHA-capped-TiO_2 nanoparticles. The diffraction pattern of TiO_2 anatase is also reported as a reference

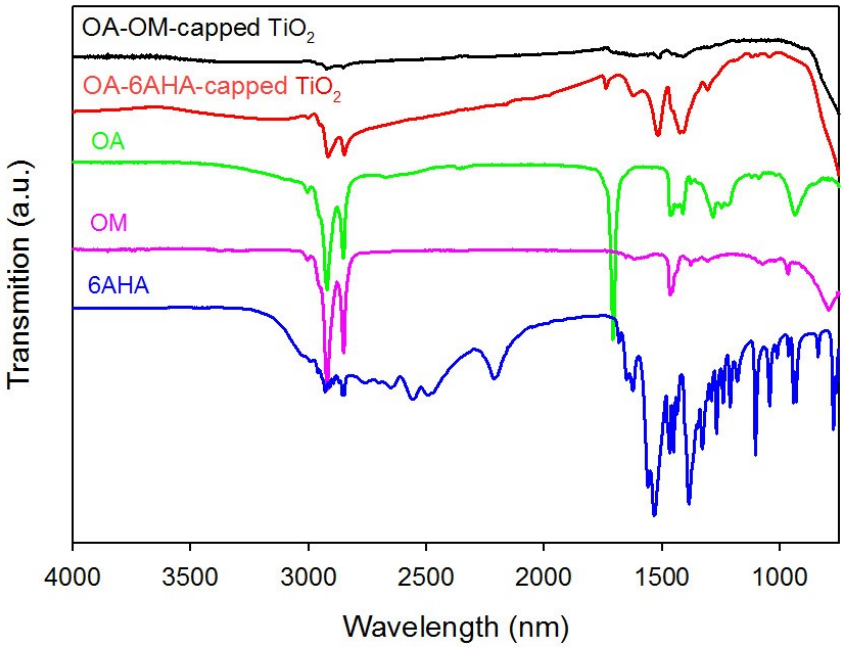

Figure 6.3. FTIR spectra of OA-OM-capped-TiO_2 (A1), OA-6AHA-capped-TiO_2 (A2) nanoparticles, pure OA, OM, and 6AHA

6.3.1.3. TGA characterization

TGA curves of capped-TiO_2 nanorods, obtained at a heating rate of 10ºC/min under O_2 atmosphere, are shown in Figure 6.4. For both surfactants combinations, an initial weight loss starting from 50ºC was observed. The most significant weight loss occured between 200 and 480ºC, which is a clear indication of the presence of surfactants OA/OM and OA/6AHA surfactants on the surface of TiO_2 nanorods. For higher temperatures (> 480ºC), the small weigh loss is attributed to the decomposition of residual product traces that forms a sheath over the TiO_2 nanoparticles.[34] By calculating the weight loss different from 200 to 480ºC, the weight proportions of OA/OM and OA/6AHA surfactants were around 9% and 16%, respectively. These results are all in agreement with those already obtained in our previous work.[21] In addition, according to the TGA spectrum, the amount of water absorbed on the surface of TiO_2 nanoparticles, which was already observed above by FTIR characterization, was around 1.4% for OA-OM-capped-TiO_2 and 3.5% OA-6AHA-capped-TiO_2.

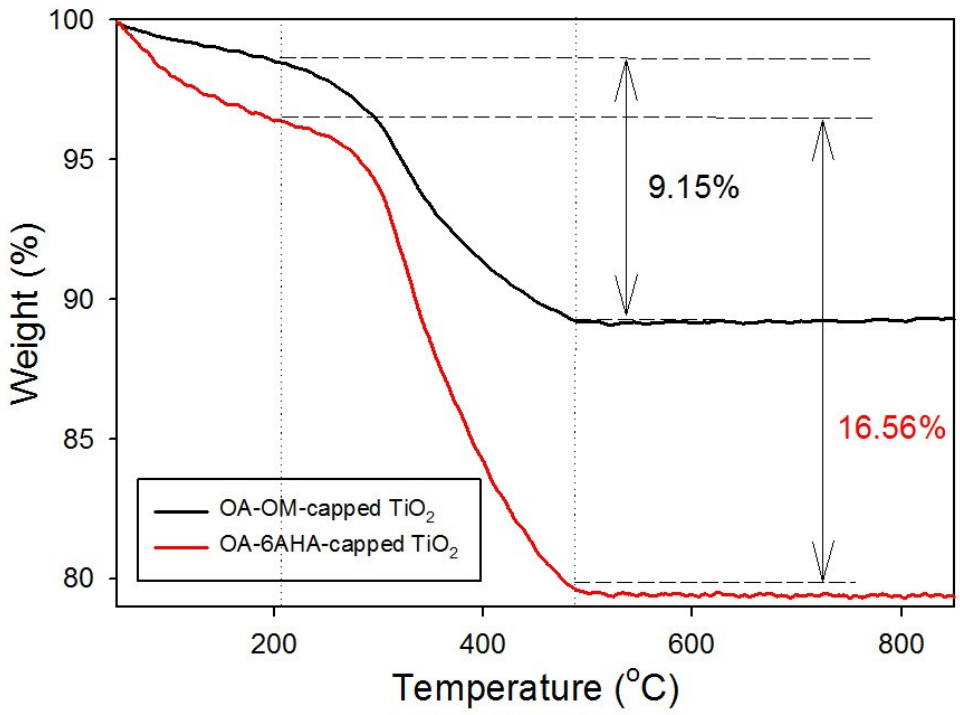

Figure 6.4. TGA spectra of OA-OM-capped-TiO_2 nanoparticles (A1) and OA-6AHA-capped-TiO_2 (A2) nanoparticles (heating rate: 10ºC/min, O_2 atmosphere)

6.3.1.4. UV-vis characterization

The UV–vis absorption spectra of both OA/OM and OA/6AHA surfactant-capped-TiO_2 nanorods are shown in Figure 6.5. As shown, their corresponding absorption band edges were around 370 and 380 nm, which are approximately similar to the gap energy of bulk anatase TiO_2 (385 nm). It is important to mention that, for small TiO_2 nanoparticles (size < 20 nm), Ti atoms at the surface of the nanoparticles adjust their coordination environment (compression of the Ti-O bond) in order to accommodate the curvature of the nanoparticles.[35] Then, the hybrid localized defect sites could enhance the selective reactivity of TiO_2 nanoparticles towards bidentate ligands binding. As a consequence, the chelation of Ti atoms on the surface with electron donating bidentate ligands changes the electronic properties of TiO_2 nanoparticles. Then, the absorption of light by the charge–transfer complex yields to the excitation of electrons from the chelating ligand directly into the conduction band of these nanoparticles.[36] By using different surfactants during the synthesis process, different capping ligands were observed to bind on the surface of TiO_2 nanoparticles, which results in different charge-transfer processes from the chelating ligand into the conduction band for the different types of TiO_2 nanoparticles. Therefore, a red shift of the UV-vis absorption spectra is expected for both OA/OM and OA/6AHA surfactant-capped- TiO_2 nanoparticles. Hence, UV-vis spectra show that the charge transportation is better for OA-6AHA-capped-TiO_2 nanoparticles than for OA-OM-capped-TiO_2 nanoparticles. The energy band gap was evaluated from the following Tauc relation:

$$(\alpha h\nu)^{1/2} \propto (h\nu - E_g) \tag{6-1}$$

where α (cm^{-1}) is the absorption coefficient, h (J.s) is the Plank constant, ν (Hz) is the frequency of radiation, and E_g (eV) is the energy band gap for direct band gap semiconductor. By drawing the tangent line on the linear part of the curve $(\alpha h\nu)^{1/2}$ versus photon energy, $h\nu$, the intercept of this line with the photon energy axis gives the value of E_g (see the insets of Figure 6.5).[37] Based on that, the energy band gaps for OA-OM-capped-TiO_2 and OA-6AHA-capped-TiO_2 nanoparticles were respectively 3.53 and 3.31 eV.

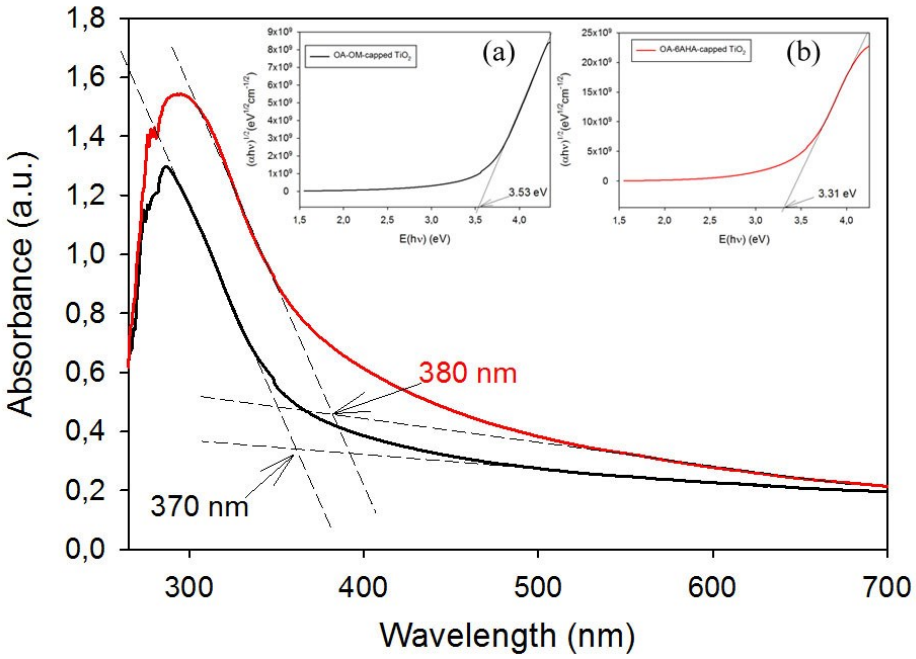

Figure 6.5. UV-vis characterization of capped-TiO_2 nanoparticles (a) OA-OM-capped-TiO_2, (b) OA-6AHA-capped-TiO_2. The insets show their respective band gap energy plots.

6.3.2. Analysis of the synthesized CdS modified TiO_2 nanorods

6.3.2.1. FTIR characterization

FTIR characterization was done for the CdS/TiO_2 nanocomposite samples in order to analyze their surface properties. Figure 6.6 shows the corresponding spectra, together with those of pure OM, OM, 6AHA and $NOBF_4$. As shown, after doing the surface treatment with $NOBF_4$ and depositing CdS on the surface of TiO_2 nanorods, the essential peak characteristics of -C-H, =C-H, -C=O-, -C-O-, and $–NH_2$ stretching vibration of the different surfactants either disappeared or appeared very weak. This is an indication that $NOBF_4$ treatment process was able to remove a big part of OA, OM and 6AHA molecules attached to TiO_2 nanorod surface.

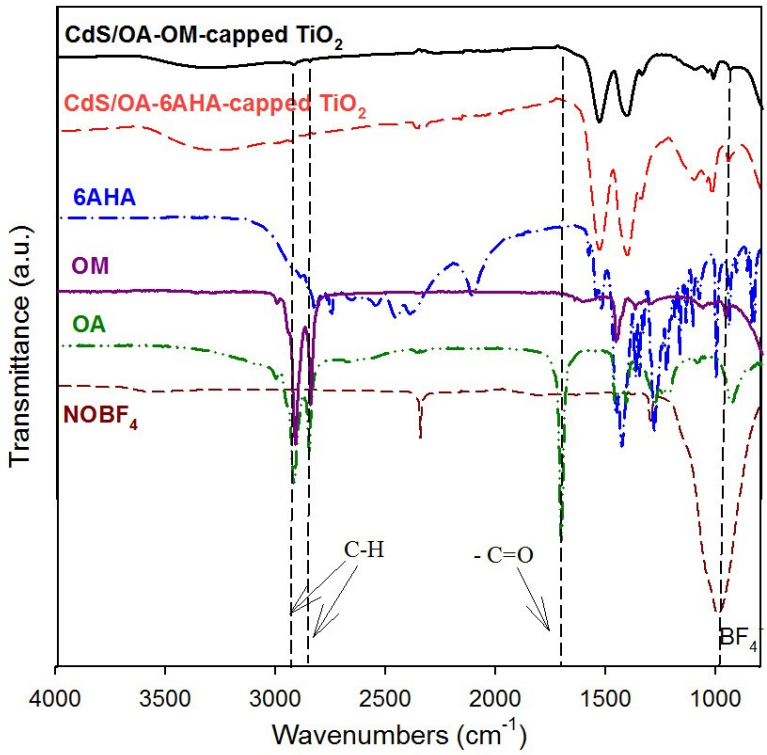

Figure 6.6. FTIR curves of the two developed CdS/TiO_2 nanocomposites, together with those of pure OA, OM, 6AHA and $NOBF_4$.

6.3.2.2. TGA characterization

Figure 6.7 shows the TGA curves of both CdS/TiO_2 nanocomposites and that of bulk CdS. The weight losses below 200ºC were attributed to water absorbed on the surface of the nanocomposites, while the weight losses from 200-480ºC were attributed to the loss of OA/OM and OA/6AHA surfactants from the surface of capped-TiO_2 nanoparticles. As shown, a non-negligible gain in mass was observed between 480 and 750°C for both CdS and CdS/TiO_2 nanocomposites. This surprising gain in mass is due to the formation of cadmium sulphate ($CdSO_4$).[38] The latter began to decompose at around 750ºC, which explains the decrease in mass observed at higher temperatures.

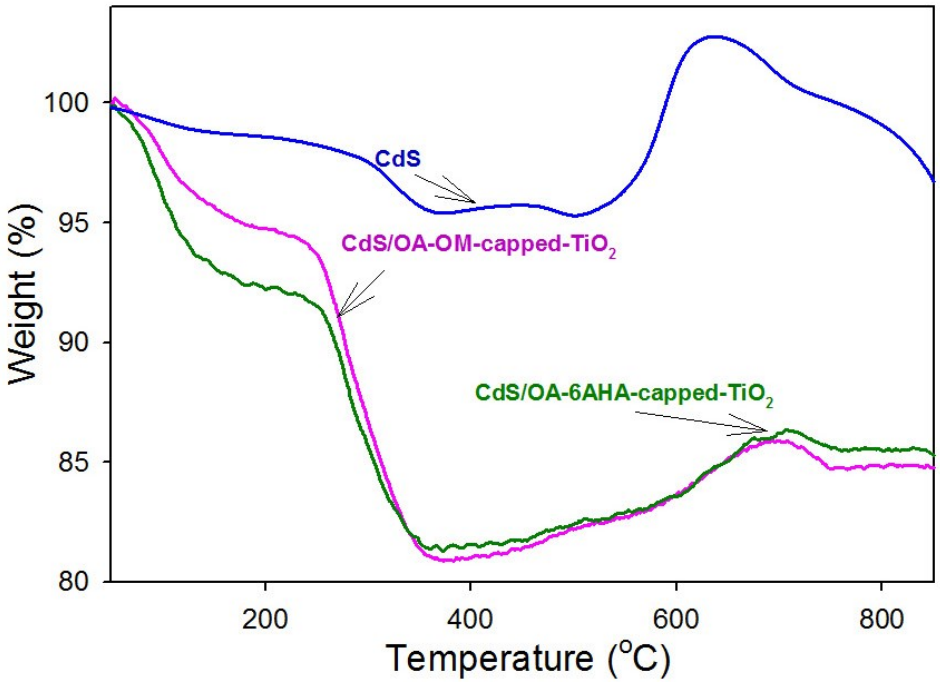

Figure 6.7. TGA spectra of CdS/OA-OM-capped-TiO_2 (A1) and CdS/OA-6AHA-capped-TiO_2 (A2) (heating rate: 10°C/min, O_2 atmosphere).

6.3.2.3. UV-vis characterization

As reported before, TiO_2 nanoparticles with their characteristic band gap of around 3.2 eV had no absorption band in the visible region. They only show a characteristic absorption spectrum (absorption of Ti–O bond) in ultraviolet light range from 320 to 400 nm. However, as clearly shown in Figure 6.8, the addition of CdS on the surface of TiO_2 nanorods can effectively shift the absorption range of TiO_2 into visible light region of 400–550 nm due to the narrow band gap of CdS (2.4 eV). Compared to the spectra of CdS and both capped-TiO_2 nanoparticles, the spectra of CdS/TiO_2 nanocomposites are basically a combination of those of CdS and capped-TiO_2, where the absorption bands around 330 nm were from TiO_2, and the broad absorption bands around 530 nm were from CdS. The red-shift of absorptions bands of the CdS/TiO_2 nanocomposites were probably due to the coupling between TiO_2 and CdS, leading to the decrease of surface defects.[39] With these shifts in absorption bands, the light-harvesting efficiencies of CdS/TiO_2 nanocomposites

were larger than those of TiO_2 nanoparticles in the visible light region, which is benefic for the photovoltaic activity. As shown, the highest was observed for CdS/OA-6AHA-capped-TiO_2 nanocomposite.

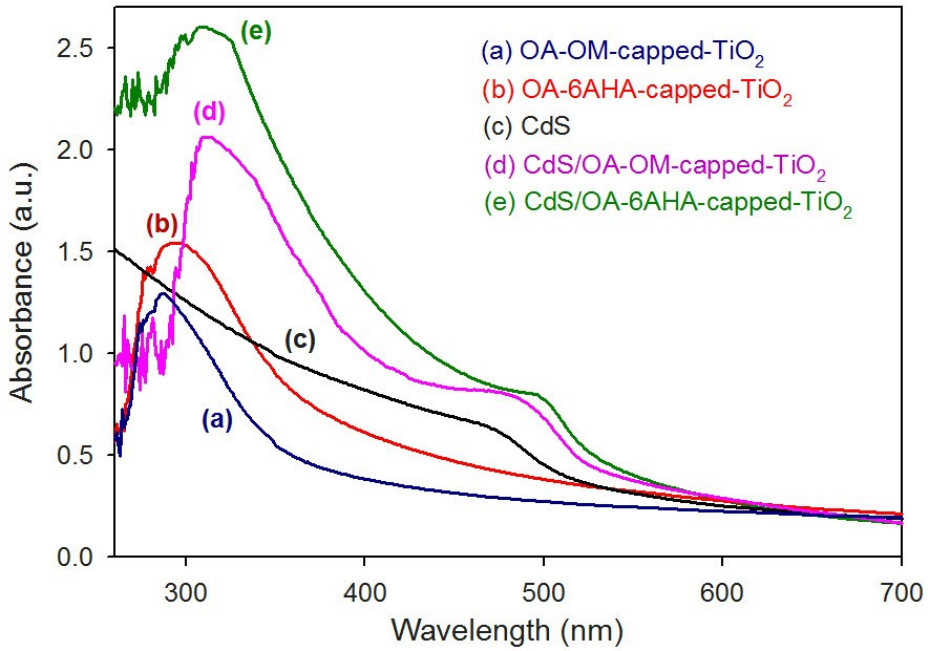

Figure 6.8. UV-vis characterization of capped-TiO_2 nanoparticles, CdS, and CdS/ TiO_2 nanocomposites.

6.3.3. Characterization of BHJSCs with active layers based on MEH-PPV/capped-TiO_2 or MEH-PPV/CdS/TiO_2

6.3.3.1. SEM characterization

Figure 6.9 shows the typical SEM cross thickness images of BHJSC devices prepared using different active layer materials (blends A1, A2, S1, and S2). BHJSC whole thickness was around 0.5µm, which is composed of 70 nm Aluminium cathode, 100 nm ITO glass, and around 330 nm of PEDOT:PSS and photoactive layers. The thickness of the photoactive layer plays an important role in the final device efficiency. It should be thick enough to absorb all the maximum incident-light but would not burden the charge

transportation. Therefore, a careful optimization of layer thicknesses is necessary to place the maximum of the optical field in the photoactive material and maximize the absorption of incident photons.[40,41]

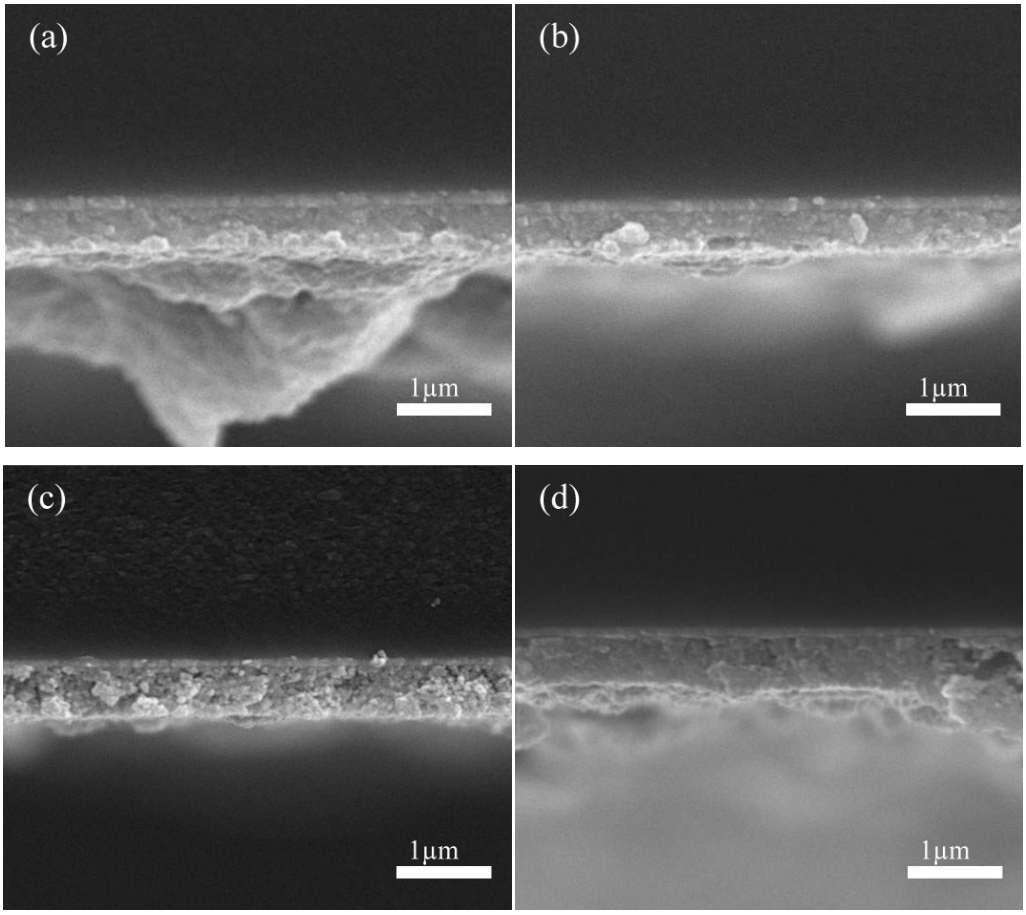

Figure 6.9. SEM pictures of BHJSC active layer blends: A1 (a), A2 (b), S1 (c), and S2 (d)

6.3.3.2. TGA characterization

The TGA characterization of MEH-PPV/capped-TiO_2 (active layer blends A1, A2) and MEH-PPV/CdS/TiO_2 (active layer blends S1 and S2) are presented in Figure 6.10. As all the blends of MEH-PPV with TiO_2 nanoparticles or with CdS/TiO_2 were prepared using the blending solution method, in which there is no chemical bonding up between two materials, their corresponding TGA curves are expected to be the combination of those of pure MEH-PPV and TiO_2 nanoparticles and CdS/TiO_2 nanocomposites. As the surfactant-

capped-TiO_2 nanorods used in blends A1 and A2 had respectively OA/OM and OA/6AHA surfactants on their surfaces, consequently the weight loss difference between the blend A1 (around 18%) and the blend A2 (around 24%) was not far from the weight loss difference between the two surfactant-capped-TiO_2 nanorods themselves (~7%). However, as shown in the figure, the TGA curves corresponding to the blends S1 and S2 show no big loss difference, due to the effective reduced residues of OA, OM and 6AHA molecules on TiO_2 nanorod surface.

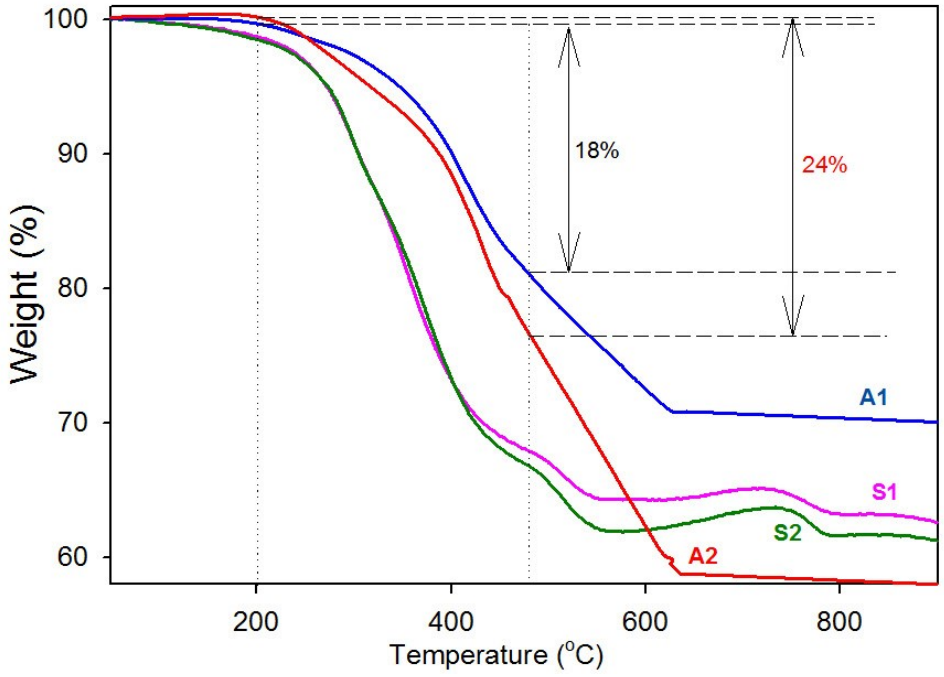

Figure 6.10. TGA spectra of BHJSC active layer blends A1, A2, and S2 (heating rate: 10°C/min, O_2 atmosphere).

6.3.3.3. UV-vis characterization

Figure 6.11 shows the UV-vis spectra of MEH-PPV/capped-TiO_2 (active layer blends A1, A2) and MEH-PPV/CdS/TiO_2 (active layer blends S1 and S2) together with the spectrum of pure MEH-PPV conjugated polymeric matrix. As shown, the UV-vis spectrum of pure MEH-PPV consists of three absorption peaks at ~500, 330 and 240 nm in the region between 220 and 800 nm. These peaks correspond to PPV-derivatives; also, the spectrum shows a sharp onset near 590 nm (2.1 eV). The absorption peak observed near 500 nm (in

the visible region) is related to the transition $\pi - \pi^*$ of the MEH-PPV conjugated polymer.[6,42] The figure shows that this peak remained at approximately the same position when MEH-PPV was blended with capped-TiO_2 nanoparticles (blends A1 and A2). However, when MEH-PPV was blended with CdS/TiO_2 nanocomposites (blends S1 and S2), this peak was broaden, red-shifted and extended to 525-530 nm range. This is due to the fact that MEH-PPV and CdS/TiO_2 nanocomposites have complementary absorption spectra and light harvesting, while the absorption spectra in the visible region of MEH-PPV/capped- TiO_2 mostly correspond to the absorption of the MEH-PPV matrix.[43] Furthermore, in the region between 300 and 750 nm, all the blends show no new peaks; the absorption is almost the overlap of their pure components, indicating no chemical bonding between the MEH-PPV matrix and capped-TiO_2 nanoparticles or CdS/TiO_2 nanocomposites.

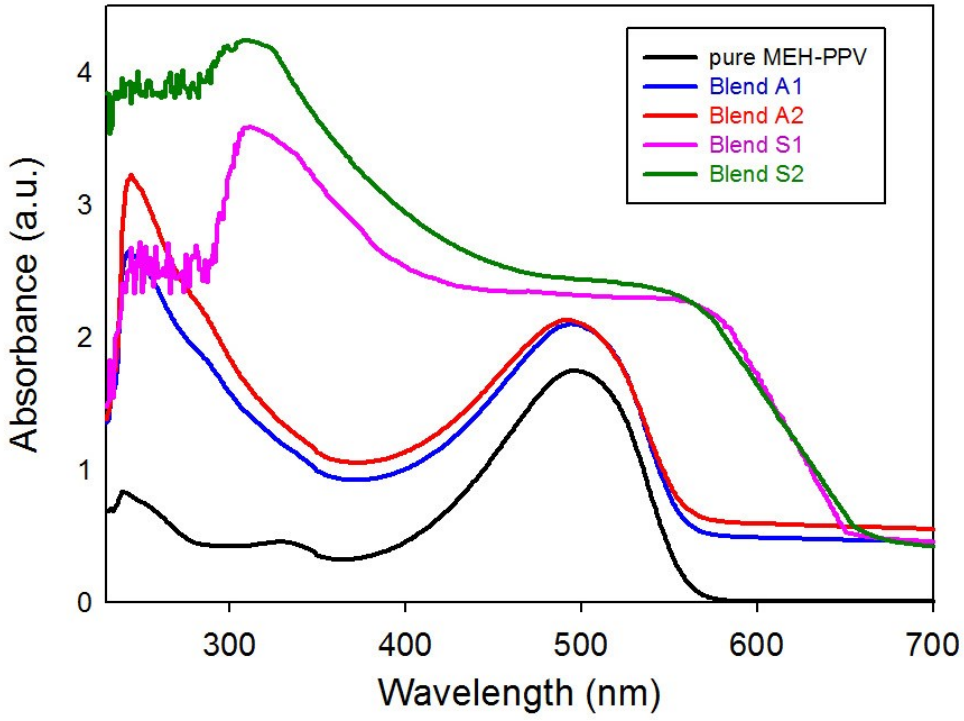

Figure 6.11. UV-vis of polymer composite of MEH-PPV and two different CdS/TiO_2 nanocomposites. MEH-PPV/OA-OM-capped-TiO_2 NPs (blend A1), MEH-PPV/OA-6AHA-capped-TiO_2 NPs (blend A2), MEH-PPV/CdS/OA-OM-capped-TiO_2 NPs (blend S1) and MEH-PPV/CdS/OA-6AHA-capped-TiO_2 (blend S2).

6.3.3.4. PL characterization

The efficiency of charge trapping and recombination of photo-induced electrons and holes in the developed composites could be verified by the PL characterization. Figure 6.12 shows the PL emission spectra for pure MEH-PPV, MEH-PPV/TiO_2 (active layer blends A1 and A2), and MEH-PPV/CdS/TiO_2 (active layer blends S1 and S2) in dichlorobenzyl at room temperature under light excitation at a wavelength of 495 nm. It can be observed that a significant quenching of the emission intensity of MEH-PPV occurs with the addition of TiO_2 nanorods or CdS/TiO_2 nanocomposites. According to PL spectra of all the samples, MEH-PPV/CdS/TiO_2 blends exhibited much weaker intensity of peaks than MEH-PPV/capped TiO_2 blends. Though the emission features of the polymer are not affected by the presence of CdS/TiO_2 nanocomposites, the significant quenching in the emission intensity could be ascribed to the effectively charge transfer from MEH-PPV to CdS then to TiO_2 surface, and also to the lower recombination probability of photo-induced electrons and holes in MEH-PPV. In addition, this degree of PL quenching is an indication of how well the nanoparticles are mixed in the polymer and the quality of the interface between the MEH-PPV matrix and the dispersed nanoparticles.[44]

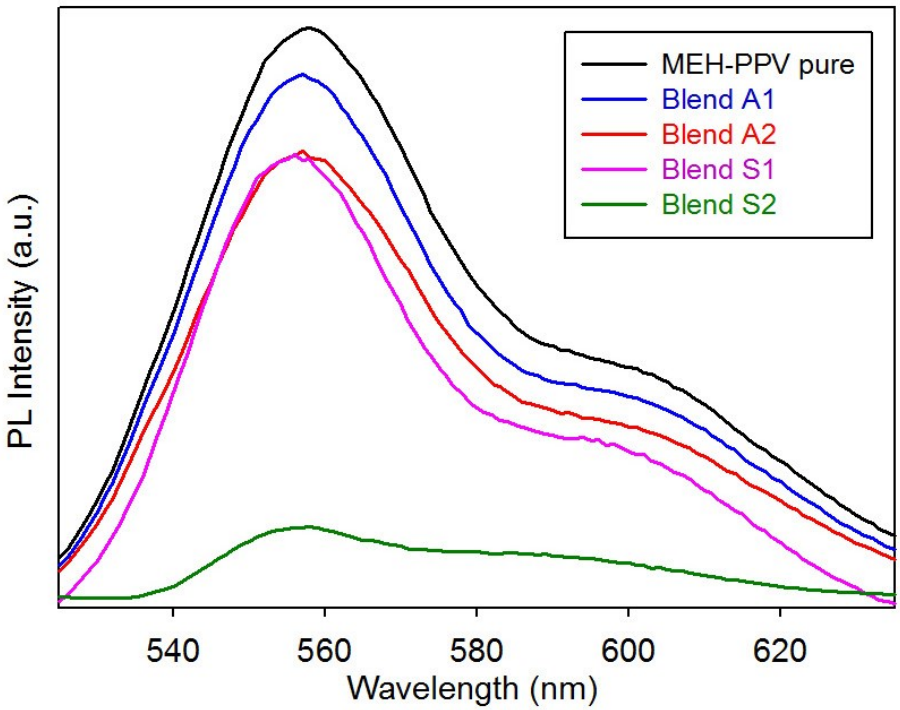

Figure 6.12. Photoluminescence (PL) of pure MEH-PPV and BHJSC active layer blends A1, A2, S1, and S2.

It is well known that surfactants are very important to stabilize and control the shape and size of TiO_2 nanorods during the synthesis step. Also, they are very useful to increase the dispersion of particles inside the polymer matrix. However, these useful surfactants could be a major hurdle to the charge transfer between the MEH-PPV matrix and TiO_2 nanorods or CdS/TiO_2 nanocomposites. As shown in Figure 6.12, the presence of different surfactants capped on the surface of TiO_2 nanorods led to a significant difference in the PL quenching of their corresponding blends. The PL quenching of the blends A2 and S2 were respectively higher than those of the blends A1 and S1. This could be due to the nature of the capping agent itself that affects the efficiency of charge transfer between TiO_2 nanoparticles and also within the nanoparticle itself. In fact, both A1 and S1 blends were based on OA-OM-capped-TiO_2 nanorods, while A2 and S2 blends S2 were based on OA-6AHA-capped-TiO_2 nanorods. Only the surfactant OM (used for A1 and S1 blends) that was replaced by 6AHA for A2 and S2 blends. The main difference between these two surfactants is that the length of the carbon-chain of 6AHA is much shorter than of that OM. It was reported in literature that carriers' mobility decreases exponentially with increasing

ligand length.[45] Hence, the probability for electrons and holes recombination is higher with using OM as surfactant rather than 6AHA due the lower carrier mobility, which explains the lower PL quenching of A1 and S1 blends compared to A2 and S2 blends.

6.3.3.5. Current density- voltage (J-V) characterization of BHJSCs

Figure 6.13 show the J-V curves under dark and under 100 mW/cm^2 (AM 1.5 G) illumination for four different BHJSC devices with the active layer composed of A1, A2, S1 and S2 blends. The corresponding photovoltaic parameters [(open-circuit voltage (V_{OC}), short-circuit current density (J_{SC}), fill factor (FF) and the PCE)] are summarized in Table 6.1. As shown by the insets of both figures, the J–V curves in the dark of all the devices pass through the origin, which is currently reported for heterojunction solar cells.

As mentioned in literature[46] for an active layer composed of MEH-PPV/TiO_2 blend, due to the fact that the work function of TiO_2 anatase is 5.1 eV, which is closed to the work function of ITO (4.8 eV) and the HOMO of MEH-PPV, the transportation of electron-holes is not effective, leading to a poor PEC. In our case, the first BHJSC device has an active layer composed of MEH-PPV blended with OA-OM-capped-TiO_2 nanorods (blend A1). This device showed a PCE of 0.003%, which is very low. When OM is replaced by 6AHA as surfactant (blend A2), the PCE was tripled. As expected from UV-vis and PL characterizations of the four blends A1, A2, S1 and S2, an increase in V_{OC}, J_{SC}, and PCE could be obtained by using an active layer composed of MEH-PPV blended with the CdS/capped-TiO_2 composite (blends S1 and S2). This increase is due to the higher efficiency of CdS compared to MEH-PPV; so more electrons from MEH-PPV would be able to travel faster to CdS.[47] Therefore, more electrons from the MEH-PPV matrix would be transported to the photoanode via CdS, TiO_2 and ITO. Moreover, the better results were observed with the S2 blend.

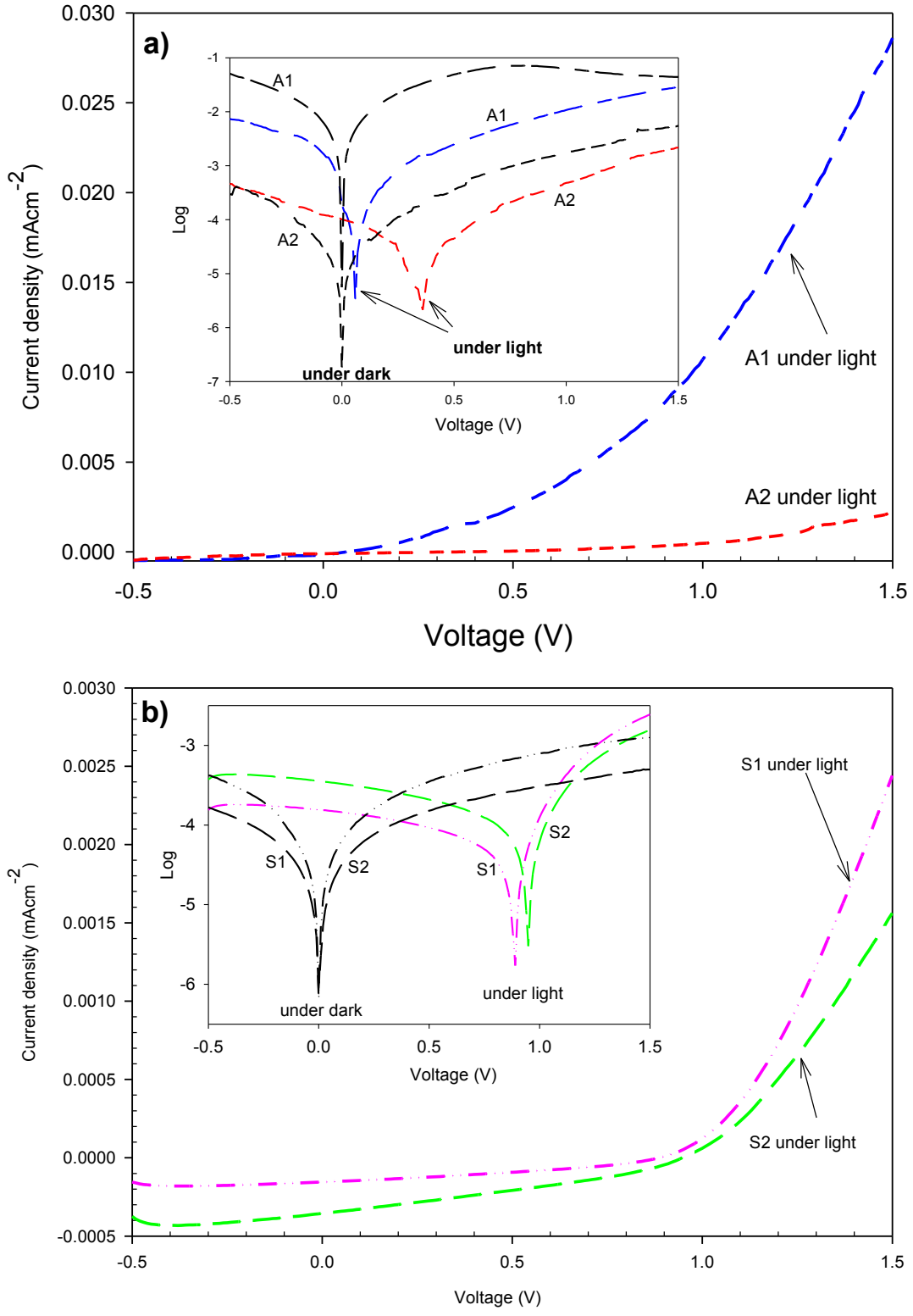

Figure 6.13. J-V Characterization under light illumination (1.5 AM) of BHJSC devices with the active layer blends (a) A1 and A2, and (b) S1 and S2. The insets are their corresponding log J–V properties in the dark and under light.

Table 6.1. Summary of the photovoltaic parameters of BHJSC devices with active layer blends A1, A2, S1, and S2

Sample ID	Active layer	Voltage (V)	Current (mA)	FF (%)	PEC (%)
A1	MEH-PPV blend with OA-OM-capped-TiO_2 (A1)	0.06	0.19	24.41	0.0028
A2	MEH-PPV blend with OA-6AHA-capped-TiO_2 (A2)	0.32	0.1	27.96	0.0090
S1	MEH-PPV blend with CdS/OA-OM-capped-TiO_2 (S1)	0.89	0.16	33.82	0.0467
S2	MEH-PPV blend with CdS/OA-6AHA-capped-TiO_2 (S2)	0.95	0.36	31.48	0.1062

6.4. Conclusion

In summary, the synthesis of TiO_2 nanorods has been proposed using OA, which is more favored to bind strongly to TiO_2 {001} faces, and OM or 6AHA that weakly bind on {101} faces. OA/OM and OA/6AHA combinations led to an oriented TiO_2 growth to form TiO_2 nanorods. The UV-vis characterization of the developed caped-TiO_2 nanorods showed that the charge carrier was better for OA-6AHA-capped-TiO_2 nanorods than for OA-OM-capped-TiO_2 nanorods due to shorter 6AHA chain length, compared to that of OM. Further optimization of the developed TiO_2 nanorods was done by doping CdS nanoparticles on TiO_2 surface. UV-vis characterization of the developed CdS/TiO_2 nanocomposites showed red-shift of absorptions bands due to the coupling between TiO_2 and CdS, which is benefic for their photovoltaic activity. When blended with MEH-PPV conjugated polymer, photoluminescence characterization showed that the developed MEH-PPV/CdS/TiO_2 blends presented improved charge transfer from MEH-PPV to TiO_2 surface.

Finally, the same trend was also observed when the MEH-PPV/capped-TiO_2 blends and MEH-PPV/CdS/TiO_2 blends were used as BHJSC active layers. The BHJSC devices made from the latter blends showed greater improvement in their PEC. This improvement

is due to the increase of electron mobility thanks to the presence of CdS quantum dots on TiO_2 surface, as mentioned above. Also, the obtained PEC results showed that the combination of OA/6AHA surfactants was better than that of OA/OM.

Acknowledgements

The authors would like to thank the Natural Sciences and Engineering Research Council of Canada (NSERC) for financial support of this work.

6.5. Reference

(1) Brabec, C. J.; Sariciftci, N. S.; Hummelen, J. C. *Adv. Funct. Mater.* **2001**, *11*, 15–26.

(2) Mihailetchi, V. D.; Koster, L. J. a.; Blom, P. W. M. *Appl. Phys. Lett.* **2004**, *85*, 970.

(3) Kim, Y.; Choulis, S. a.; Nelson, J.; Bradley, D. D. C.; Cook, S.; Durrant, J. R. *Appl. Phys. Lett.* **2005**, *86*, 063502.

(4) Wang, L.; Liu, Y.; Jiang, X.; Qin, D.; Cao, Y. *J. Phys. Chem. C* **2007**, *111*, 9538–9542.

(5) Kang, Y.; Kim, D. *Sol. Energy Mater. Sol. Cells* **2006**, *90*, 166–174.

(6) Ram, M. K.; Sarkar, N.; Bertoncello, P.; Sarkar, A.; Narizzano, R.; Nicolini, C. *Synth. Met.* **2001**, *122*, 369–378.

(7) Verma, D.; Ranga Rao, A.; Dutta, V. *Sol. Energy Mater. Sol. Cells* **2009**, *93*, 1482–1487.

(8) Wu, M.-C.; Lo, H.-H.; Liao, H.-C.; Chen, S.; Lin, Y.-Y.; Yen, W.-C.; Zeng, T.-W.; Chen, Y.-F.; Chen, C.-W.; Su, W.-F. *Sol. Energy Mater. Sol. Cells* **2009**, *93*, 869–873.

(9) Al-Ibrahim, M.; Roth, H.-K.; Zhokhavets, U.; Gobsch, G.; Sensfuss, S. *Sol. Energy Mater. Sol. Cells* **2004**, *85*, 13–20.

(10) Shiga, T.; Takechi, K.; Motohiro, T. *Sol. Energy Mater. Sol. Cells* **2006**, *90*, 1849–1858.

(11) Zhou, Y.; Riehle, F. S.; Yuan, Y.; Schleiermacher, H.; Niggemann, M.; Urban, G. a.; Krüger, M. *Appl. Phys. Lett.* **2010**, *96*, 013304.

(12) Zarazúa, I.; De la Rosa, E.; López-Luke, T.; Reyes-Gomez, J.; Ruiz, S.; Ángeles Chavez, C.; Zhang, J. Z. *J. Phys. Chem. C* **2011**, *115*, 23209–23220.

(13) Huynh, W. U.; Dittmer, J. J.; Alivisatos, a P. *Science* **2002**, *295*, 2425–2427.

(14) Olson, D. C.; Piris, J.; Collins, R. T.; Shaheen, S. E.; Ginley, D. S. *Thin Solid Films* **2006**, *496*, 26–29.

(15) Wang, M.; Wang, X. *Sol. Energy Mater. Sol. Cells* **2008**, *92*, 766–771.

(16) Roberson, L. B.; Poggi, M. A.; Kowalik, J.; Smestad, G. P.; Bottomley, L. A.; Tolbert, L. M. *Coord. Chem. Rev.* **2004**, *248*, 1491–1499.

(17) Balis, N.; Dracopoulos, V.; Stathatos, E.; Boukos, N.; Lianos, P. *J. Phys. Chem. C* **2011**, *115*, 10911–10916.

(18) Slooff, L. H.; Wienk, M. M.; Kroon, J. M. *Thin Solid Films* **2004**, *451-452*, 634–638.

(19) Zhou, Y.; Li, Y.; Zhong, H.; Hou, J.; Ding, Y.; Yang, C.; Li, Y. *Nanotechnology* **2006**, *17*, 4041–4047.

(20) Acharya, K. P.; Hewa-Kasakarage, N. N.; Alabi, T. R.; Nemitz, I.; Khon, E.; Ullrich, B.; Anzenbacher, P.; Zamkov, M. *J. Phys. Chem. C* **2010**, *114*, 12496–12504.

(21) Vu, T. T. D.; Mighri, F.; Do, T.-O.; Ajji, A. *J. Nanosci. Nanotechnol.* **2012**, *12*, 2815–2824.

(22) Vu, T. T. D.; Mighri, F.; Ajji, A.; Do, T. *Ind. Eng. Chem. Res.* **2014**, *53*, 3888–3897.

(23) Liu, J.; Wang, W.; Yu, H.; Wu, Z.; Peng, J.; Cao, Y. *Sol. Energy Mater. Sol. Cells* **2008**, *92*, 1403–1409.

(24) Joo, J.; Kwon, S. G.; Yu, T.; Cho, M.; Lee, J.; Yoon, J.; Hyeon, T. *J. Phys. Chem. B* **2005**, *109*, 15297–15302.

(25) Li, X.-L.; Peng, Q.; Yi, J.-X.; Wang, X.; Li, Y. *Chemistry* **2006**, *12*, 2383–2391.

(26) Jun, Y.-W.; Casula, M. F.; Sim, J.-H.; Kim, S. Y.; Cheon, J.; Alivisatos, A. P. *J. Am. Chem. Soc.* **2003**, *125*, 15981–15985.

(27) Chen, S.; Liu, W. *Mater. Chem. Phys.* **2006**, *98*, 183–189.

(28) Chen, M.; Feng, Y.-G.; Wang, X.; Li, T.-C.; Zhang, J.-Y.; Qian, D.-J. *Langmuir* **2007**, *23*, 5296–5304.

(29) Limaye, M. V; Singh, S. B.; Date, S. K.; Kothari, D.; Reddy, V. R.; Gupta, A.; Sathe, V.; Choudhary, R. J.; Kulkarni, S. K. *J. Phys. Chem. B* **2009**, *113*, 9070–9076.

(30) He, J.; Kanjanaboos, P.; Frazer, N. L.; Weis, A.; Lin, X.-M.; Jaeger, H. M. *Small* **2010**, *6*, 1449–1456.

(31) Si, H.; Wang, H.; Shen, H.; Zhou, C.; Li, S.; Lou, S.; Xu, W.; Du, Z.; Li, L. S. *CrystEngComm* **2009**, *11*, 1128.

(32) Raupach, M. *Clays Clay Miner.* **1976**, *24*, 127–133.

(33) Nguyen, T.; Mrabet, D.; Vu, T.-T.-D.; Dinh, C.-T.; Do, T.-O. *CrystEngComm* **2011**, *13*, 1450.

(34) Tzitzios, V.; Niarchos, D.; Margariti, G.; Fidler, J.; Petridis, D. *Nanotechnology* **2005**, *16*, 287–291.

(35) Chen, L. X.; Rajh, T.; Jäger, W.; Nedeljkovic, J.; Thurnauer, M. C. *J. Synchrotron Radiat.* **1999**, *6*, 445–447.

(36) Persson, P.; Bergström, R.; Lunell, S. *J. Phys. Chem. B* **2000**, *104*, 10348–10351.

(37) Murphy, A. *Sol. Energy Mater. Sol. Cells* **2007**, *91*, 1326–1337.

(38) Sabah, A.; Siddiqi, S. A.; Ali, S. *World Acad. Sci. Eng. Tech.* **2010**, *45*, 82–89.

(39) Wang, C. L.; Zhang, H.; Zhang, J. H.; Li, M. J.; Sun, H. Z.; Yang, B. *J. Phys. Chem. C* **2007**, *111*, 2465–2469.

(40) Günes, S.; Neugebauer, H.; Sariciftci, N. S. *Chem. Rev.* **2007**, *107*, 1324–1338.

(41) Adikaari, A. A. D. T.; Dissanayake, D. M. N. M.; Silva, S. R. P. *IEEE J. Sel. Top. Quantum Electron.* **2010**, *16*, 1595–1606.

(42) Kim, S.-S.; Jo, J.; Chun, C.; Hong, J.; Kim, D. *J. Photochem. Photobiol. A Chem.* **2007**, *188*, 364–370.

(43) Yang, B. D.; Yoon, K. H.; Chung, K. W. *Mater. Chem. Phys.* **2004**, *83*, 334–339.

(44) Salafsky, J. *Phys. Rev. B* **1999**, *59*, 10885–10894.

(45) Liu, Y.; Gibbs, M.; Puthussery, J.; Gaik, S.; Ihly, R.; Hillhouse, H. W.; Law, M. *Nano Lett.* **2010**, *10*, 1960–1969.

(46) Xiong, G.; Shao, R.; Droubay, T. C.; Joly, a. G.; Beck, K. M.; Chambers, S. a.; Hess, W. P. *Adv. Funct. Mater.* **2007**, *17*, 2133–2138.

(47) Greenham, N. C.; Peng, X.; Alivisatos, A. P. *Phys. Rev. B* **1996**, *54*, 628–637.

.

Chapter 7. Conclusion

7.1. General conclusions

During the course of this research work, a number of conclusions have been reached, regarding the preparation, characterization and utilization of TiO_2 based photocatalysts in the H_2 production via water splitting and in BHJ solar cells. In addition, recommendations and suggestions for future work in the area of photocatalytic hydrogen production and photovoltaic are also evaluated.

Firstly, we recommended a new simple synthesis routine using solvothermal method in autoclave at low temperature to synthesize TiO_2 nanoparticles. The shape and size of those TiO_2 NPs were able to be controlled just by adjusting the reaction condition, especially the capping agents. In details, by varying the presence of different capping agents, which include oleic acid, oleylamine, and amino 6-aminohexanoic acid, we achieved anatase TiO_2 NPs with shape of sphere, rod, and rhombic; and with size of nanorod from 3 x 40 nm to 3 x 20 nm. Based on that, the effects of capping agent on the TiO_2 particles morphologies as well as optical properties were studied, analyzed and understood.

Secondly, following the first step of the study, in order to enhance the optical properties of TiO_2 NPs in visible light region, we proposed a two-step-synthesis process to deposit CdS nanoparticles on the surface of TiO_2 nanorods: steps (i) the surface properties of the achieved TiO_2 nanorods were modified by surfactant exchange with nitrosonium tetrafluoroborate ($NOBF_4$) in the direction to promote the hydrophilic properties of nanorods. (ii) CdS NPs were then deposited on surface of $NOBF_4$-TiO_2 nanorods. Several optical characterizations was done for CdS/TiO_2 and it showed that the nanocomposite has a great potential for the application both in photocatalyst H_2 production via water splitting and in BHJ solar cells, especially in visible light region.

In chapter 4, we presented the application potential of achieved CdS/TiO_2 nanocomposite in photocatalyst H_2 production via water splitting. Based on CdS/ OA-6AHA-capped-TiO_2, Ni clusters were selectively deposited on surface of nanocomposite surface as cocatalyst. Under visible-light illumination and due to the fact that electron-hole

separation was highly enhanced, the developed CdS/TiO_2 -Ni photocatalyst showed a high photocatalytic performance for the H_2 production via water splitting using ethanol as a sacrificial agent, which was around 44 times higher than that of Ni-CdS. With the coupling with TiO_2, the system appeared to be resistant to photo-corrosion, which usually was a concern when using photocatalyst that contains CdS particles. The photocatalytic activity of the system can be expected to run up to 15h of reaction.

Potential application of TiO_2 NPs and their CdS/TiO_2 nanocomposite in BHJ solar cells was demonstrated in chapter 6 and showed very promising results. The power efficiency conversion (PCE) of devices using active layer of MEH-PPV and CdS/OA-6AHA-capped-TiO_2 or CdS/OA-OM-capped-TiO_2 nanocomposites were reported to increase 11.9 and 16.7 times compare to device using active layer combine of MEH-PPV and only OA-6AHA-capped-TiO_2 NPs or OA-OM-capped-TiO_2, respectively. In this demonstration, the BHJ device architecture was designed, optimized and fabricated using the available and simplest method in the laboratory, include solution blending, photolithography, spin-coating, and thermal evaporation. The advantage of the device architecture is that photogenerated charges can be collected by the electrodes easily due to direct pathways. Where else the active layer, which is the most important layer of BHJ solar cells, was combined of MEH-PPV conjugated polymer and TiO_2 nanorods or TiO_2-based nanocomposites.

Finally, the effects of different capping agents (OA/OM and OA/6AHA) on properties of BHJ solar cells based on TiO_2 NPs and their CdS/TiO_2 nanocomposite were carefully studied in chapter 5 and 6. The work presented in chapter 5 found that the amount of OA and OM capping agents used in synthesis process have effects on the shape and surface properties of TiO_2 NPs. As resulted, the capping agent posed many effects on the energy bandgap and also on the dispersion quality of MEH-PPV/TiO_2 nanocomposites. Among those three different morphologies of OA-OM-capped-TiO_2 achieved, TiO_2 nanorods were found to have higher surface-to-volume ratio, higher delocalization of carriers, and sufficient amount of surfactant capped on surface of particles compared to TiO_2 nanosphere and TiO_2 nanorhombic. Though they helped to increase the probability of charge transfer at polymer-NPs interface, and helped to prevent the back recombination of

holes in MEH-PPV matrix and electrons in TiO_2 NPs. Therefore, TiO_2 nanorods were reported to be the most efficient for utilizing in BHJ solar cells.

In chapter 6, further studies were focused on the evaluation of effects of different surfactants on photovoltaic PCE of BHJ solar cells. The results showed that the PCE increase 3.2 times when using OA-6AHA-capped-TiO_2 nanorods (PCE = 0.009%) instead of using OA-OM-capped TiO_2 nanorods (PCE = 0.0028%). The better in PCE was explained due to the capping agent factor, in which the length of carbon-chain of 6AHA is much shorter than of OM. The carrier mobilities were reported to be decrease exponentially with increasing ligand length, hence with the usage of OM, the electron and holes would be very fast recombination before effectively transferred from MEH-PPV to TiO_2, as resulted, the lower PCE was expected. However, the poor photovoltaic response of MEH-PPV and TiO_2 NPs could be ascribed due to the surfactant NPs, which may prevent such kind of loss in charge separation in these particular types of devices. In agreement, PCE of BHJ using CdS/OA-6AHA-capped-TiO_2 was 2.3 times higher compares to the device using when using CdS/OA-OM-capped-TiO_2 nanocomposites.

7.2. Prospects

There are several directions that can be further pursued in the future:

1. Further study the effects of many other different capping agents (for example n-octyl-phosphonic acid, thiophenol, pyridyl, etc) on the performance of TiO_2 and its derivatives in BHJ solar cells and in H_2 production via water splitting.
2. Further investigate the electron-hole separation, recombination and transportation mechanism between TiO_2 and another smaller band gap energy semiconductor, in order to optimize their application in photocatalyst water splitting as well as in BHJ solar cells.
3. Further study the effects of TiO_2-based nanocomposite which compounds of surfactant-capped-TiO_2 and other metal chalcogenides on PEC of BHJ solar cells.
4. Combine surfactant-capped-TiO_2 with different chemical compositions such as carbon nanotube, N-doped GaN-Zn, etc. to enhance their photocatalytic activity.